

Role of Rydberg States In High-order Harmonic Generation

S. Beaulieu^{1,2}, D.Descamps¹, A.Comby¹, V.Wanie^{1,2}, S.Petit¹, F.Légaré², F.Catoire¹ Y.Mairesse¹

¹Université de Bordeaux - CNRS - CEA, CELIA,
UMR5107, F33405 Talence, France

² Institut National de la Recherche Scientifique,
Centre EMT, J3X1S2, Varennes, Quebec, Canada

(Dated: December 3, 2024)

The role of Rydberg states in strong field physics has known a renewed interest in the past few years with the study of resonant high-order harmonic generation. In addition to its fundamental interest, this process could create bright sources of coherent vacuum and extreme ultraviolet radiation with controlled polarization state. We investigate the spectral, spatial and temporal characteristics of the radiation produced near the ionization threshold of argon by few-cycle laser pulses. The intensity-dependence of the emission shows that two different pathways interfere to populate the Rydberg states. Furthermore, we show that the population of Rydberg states can lead to different emission mechanisms: either direct emission through XUV Free Induction Decay, or sequentially with absorption of additional photons, in processes similar to resonance-enhanced multiphoton above-threshold ionization. Last, using the attosecond lighthouse technique we show that the resonant emission from Rydberg states is not temporally confined on the attosecond timescale.

High-order Harmonic Generation (HHG) results from the interaction between a strong laser field and atoms or molecules. This extremely non-linear process can be understood as a three step mechanism [1–3]. First, an electron wavepacket (EWP) is created by strong-field ionization. The EWP is then accelerated in the ion continuum by the driving laser. Last, it can radiatively recombine with the parent ion, leading to the coherent emission of extreme ultraviolet (XUV) photons. This model successfully describes the main characteristics of the harmonic emission well above the ionization threshold, where the influence of the ionic potential on the electron wavepacket dynamics can often be neglected [4]. However, below and near the ionization threshold, the HHG mechanism becomes more complex and requires a description that goes beyond this approximation.

A particularly important and debated question is the role of resonances in HHG. Above the ionization threshold, autoionizing states and shape resonances have been shown to induce enhancement of the harmonic emission yield [5–7], to exhibit a spectral phase jump across the resonance [8, 9] and to lead to strong polarization state variations when driven with elliptically polarized light [10]. Below the ionization threshold, Chini *et al.* have observed narrow-band enhancement of the harmonic emission by atomic resonances (Rydberg states) [11]. They also demonstrated that the emission yield showed the same ellipticity dependence as the above-threshold harmonics, and suggested that polarization gating techniques [12] could thus be employed to temporally confine this emission. On the other hand, a recent theoretical study by Camp *et al.* demonstrated that the narrow-band emission below the ionization threshold emerged for long-lived dipoles which coherently emit radiation for times much longer than the pulse duration [13]. This process can be seen as XUV Free Induction Decay (xFID)

[14]. The temporal confinement of the emission from Rydberg states is thus a debated question. It is of particular importance since it could be useful to produce quasi-circularly polarized ultrashort XUV pulses [10]. The extension of the concept of FID, which was first introduced in Nuclear Magnetic Resonance [15] and later extended to the optical regime [16], to the VUV and XUV spectral range is also fundamentally very interesting.

In this letter, we experimentally investigate the role of Rydberg resonances in HHG from argon atoms. We identify xFID emission associated to the excitation of $[Ne]3s^23p^6 \rightarrow [Ne]3s^23p^5ns$ and $[Ne]3s^23p^5nd$ Rydberg series. Compared to non-resonant above threshold harmonics, the xFID emission depicts an unusual non-monotonic power scaling, as well as a larger divergence, which increases rapidly with laser intensity. We show that the Rydberg electrons can be further excited to the continuum by absorption of an even number of additional photons, resulting in a new type of above-threshold resonant-enhanced multiphoton emission (REMPE). To investigate the temporal properties of the different XUV emission mechanisms, we use the attosecond lighthouse technique [17]. While the below- and above-threshold non-resonant harmonics show clear sub-cycle confinement, the xFID shows no sign of attosecond structure.

For the experiment we used the AURORE laser system at CELIA which delivers 8 mJ, 28 fs pulses at 1 kHz repetition rate. We focused up to 4 mJ into a 1.5 m long stretched hollow core fiber (500 μm diameter, Few Cycle inc.) filled with a pressure gradient of argon (0-400 mbar) to broaden the spectrum (~ 650 -950nm tail-to-tail) through self-phase modulation. Six pairs of chirped mirrors ($-50 fs^2$ per bounce, Ultrafast Innovations) were used to compensate the group delay dispersion. A single-shot, in-line ultrabroadband second-order autocorrelator (FemtoEasy) was used to measure the pulse duration,

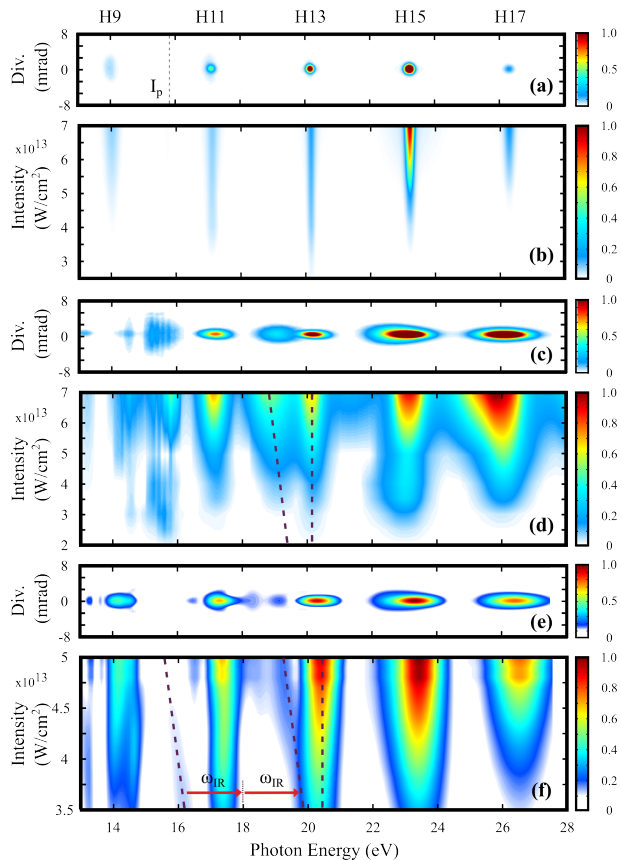


FIG. 1. (a) Spatially resolved HHG spectrum using 28 fs laser pulses ($I = 4.8 \times 10^{13} \text{ W/cm}^2$). (b) Intensity dependence of HHG spectra using 28 fs pulses. (c) Spatially resolved HHG spectrum using 7 fs laser pulses ($I = 5.2 \times 10^{13} \text{ W/cm}^2$). (d) Intensity dependence of HHG spectra using 7 fs pulses. (e) TDSE calculation of spatially resolved HHG spectrum using 7 fs laser pulse ($I = 5.0 \times 10^{13} \text{ W/cm}^2$). (f) TDSE calculation of the intensity dependence of HHG spectra.

which was optimized by linear propagation through a pair of fused silica wedges to reach 7 fs. The pulse energy was varied by rotating a zero order superachromatic half-wave plate (Fichou) in front of a broadband polarizer (FemtoLaser). For the attosecond lighthouse experiment, we placed a pair of misaligned wedges to induce a spatial chirp in the beam. The few-cycle pulses were sent under vacuum and focused by a $f=37.5$ cm spherical mirror into a $250 \mu\text{m}$ thick effusive Ar gas jet to generate high harmonics. The XUV radiation was analyzed by a flat-field XUV spectrometer, consisting of a 1200 grooves/mm holographic cylindrical grating with variable groove spacing (Shimadzu) and a set of dual microchannel plates coupled to a fast P46 phosphor screen (Hamamatsu) enabling single shot measurements. A 12-bit cooled CCD camera (PCO) recorded the spatially-resolved harmonic spectrum.

Figure 1(a) shows the harmonic spectrum obtained us-

ing 28 fs laser pulses. The spectrum is constituted of a comb of narrow, equally spaced odd harmonics, separated by twice the laser frequency $2\omega_{IR} = 3.1\text{eV}$. The field-free ionization potential of Argon (15.76 eV) lies in between harmonic 9 and 11, and these two harmonics show rather similar spectral and spatial characteristics. The evolution of the spatially-integrated harmonic spectrum is shown in Fig. 1(b) as the laser intensity increases from 2.5 to $7.0 \times 10^{13} \text{ W/cm}^2$. There is no sign of any resonant enhancement of the harmonic emission. This is because the bandwidth of the laser pulses does not enable any multiphoton resonant transition between the ground state and an excited bound state. When broadband 7 fs laser pulses are used, new structures appear in the harmonic spectrum (Fig. 1(c)): a series of narrow spectral lines between 14.2 and 15.7 eV, and a broad peak around 19 eV. These two components show spatial profiles wider than the adjacent non-resonant high-order harmonics. Varying the laser intensity from 2.0 to $7.0 \times 10^{13} \text{ W/cm}^2$ (Fig. 1(d)) shows that the narrow-bandwidth structures appear at very low intensity and do not exhibit any Stark-Shift. The peak around 19 eV is only visible when the laser intensity is above $3.5 \times 10^{13} \text{ W/cm}^2$. It shows a linear spectral shift as the intensity increases, with a slope of $\sim -1.2 \times 10^{-11} \text{ meV/W} \cdot \text{cm}^2$.

What is the origin of these two resonant components? The narrow structures below the ionization threshold are clearly associated to emission from Rydberg states, as recently predicted [13]. Because the excitation mechanism is coherent, all atoms in the medium decay in phase to the ground state by spontaneous emission, resulting in coherent emission referred to here as xFID. In the XUV range, xFID has recently been identified in the case of excitation of Rydberg and Fano resonances by an XUV beam [14]. The emission process is similar here, the difference being that multiple IR photons are absorbed to populate the excited states. The coherence of the xFID process explains the colimated nature of the XUV emission in the measurements. Since the lifetime of the Rydberg states is much longer than the IR pulse duration, the xFID mostly takes place after the generating laser pulse is over. The xFID emission thus occurs at photon energies corresponding to the field-free resonance energies. As the laser intensity increases, the Stark-shift brings lower Rydberg states into resonance, leading to the emergence of new spectral lines around 14.2 eV.

The second unusual component in the harmonic spectrum is located around 19 eV, i.e. $\sim 2\hbar\omega_0 = 3.1 \text{ eV}$ above the Rydberg states. Its spectral shift with intensity indicates that the emission is dominated by a resonant process that occurs when the laser field is on. These observations suggest a Resonance-Enhanced Multiphoton Emission (REMPE) process, similar to REMPI ionization. During the laser pulse, the electrons in the Stark-shifted Rydberg states can get further excited by absorption of 2 additional photons. They reach the ion-

ization continuum and subsequently radiatively recombine with the atomic ground state, emitting light around $E_R^{(S)} + 2\hbar\omega_0 \approx 19$ eV, where $E_R^{(S)}$ is the Stark-shifted Rydberg states energy. The spatially wider shape on the red wing of harmonic 15 is the signature of a REMPE involving two additional photons to reach $E_R^{(S)} + 4\hbar\omega_0 \approx 22$ eV. At the highest laser intensity (7×10^{13} W/cm²), this component exhibits a larger spectral shift and ends up in between H13 and H15 (Fig 1(d)). This REMPE mechanism from Rydberg states, which can create multiple harmonic frequency combs, is a new interesting strong field phenomenon which could lead to the generation of attosecond pulse train with novel temporal proprieties [18].

The fact that the REMPE emission shifts towards lower energies as the laser intensity increases is counter-intuitive, since the ac-Stark-shift pushes the Rydberg states toward higher energies. In order to confirm the assignment of the HHG spectrum and understand this effect, we performed quantum mechanical simulations. First, the single atom response was calculated solving the 1D TDSE in the velocity gauge, using a soft core potential with the Argon asymptotic Coulomb tail and ionization potential. The calculation was performed using a 7 fs FWHM gaussian envelop of the field, and repeated for different peak intensities. Second, the macroscopic signal was calculated by defining a gaussian spatial distribution of the laser intensity. The spatially resolved far-field harmonic spectrum was obtained by calculating the Hankel transform of the near-field dipole distribution. This calculation neglects longitudinal phase matching effects, which is justified by the thin nature of the gas jet used in the experiment. Fig. 1(e) shows the calculated spatially resolved HHG spectrum at 5×10^{13} W/cm² and Fig. 1(f) represent the HHG spectrum as a function of laser intensity. Remarkably, the structure at ~ 19 eV and the broadening of the red wing of H15 show up in the simulated spectrum. Looking at Fig. 1(f), we see that the REMPE peak experiences a spectral redshift as the laser intensity increase, as in the experiment (slope $\sim -2.9 \times 10^{-11}$ meV/W · cm²). A redshift with the same slope is also seen $\sim 2\hbar\omega_0$ lower in energy, which corresponds the direct emission from Rydberg states during the laser pulse. This observation suggests a Stark-shift-assisted redistribution of Rydberg population towards lower energies as the laser intensity increases, as seen in experimental Fig. 1(f)), followed by absorption of two IR photons. We performed the same simulation using a screened Coulomb potential which does not support any Rydberg state, and found that these spectral features vanished. This confirms the role of Rydberg states in the REMPE mechanism. The slope of the REMPE peak position is 2.4 times larger than the measured one. This lack of quantitative agreement is not surprising because the Stark-shift strongly depends on the Rydberg state energy, symmetry

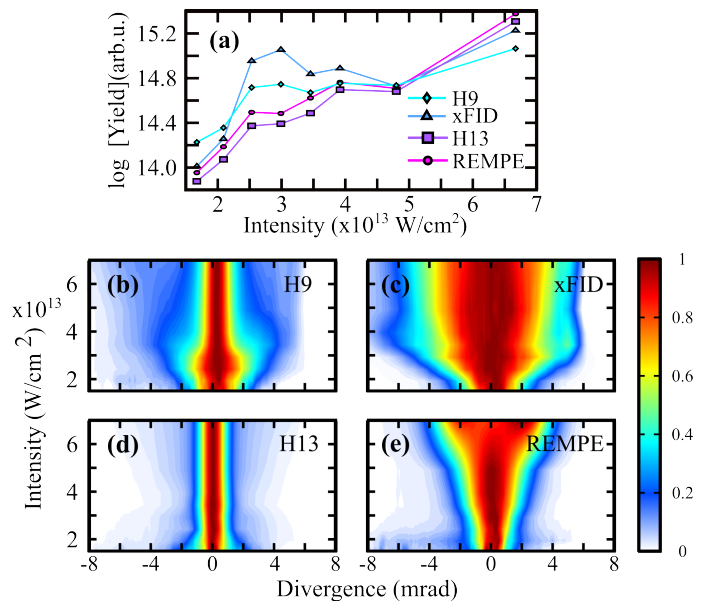


FIG. 2. (a) Intensity scaling of H9, xFID, H13 and REMPE emission yield. (b) to (e): Intensity dependence of the divergence for (b) H9, (c) xFID, (d) H13, (e) REMPE. Note that the observed saturation of the xFID divergence as a function of intensity in (c) is due to a limited numerical aperture in the experiment.

and dipole moment, which is not accurately described by the 1D model.

To obtain a deeper insight into the different emission mechanisms at play in the experiment, we monitor the intensity-dependence of the total signal from different spectral components: below threshold harmonic (H9), xFID, REMPE and above-threshold harmonic (H13) (Fig. 2). The H9 exhibits a step-growth intensity dependence, in agreement with previous investigations of below-threshold harmonics [19–21]. This effect has been explained as the result of an interference between two emission mechanisms: (i) a pure multiphoton excitation process without ionization; (ii) a rescattering process, in which long electron trajectories return to the parent ion with negative total energy and recombine to emit photons below the ionization threshold [19, 22]. Interestingly, the xFID has a similar non-monotonic behavior, and even shows a more pronounced local maximum. This suggests that the Rydberg states can be populated by two interfering processes: (i) direct multiphoton excitation from the ground state [21, 23]; (ii) tunneling of electrons and trapping by the Coulomb potential, a process referred to as Frustrated Tunnel Ionization (FTI) [24, 25]. To confirm this hypothesis, we performed similar measurements using a weak 400 nm laser beam, populating the Rydberg states through resonant 5 photon absorption. This case corresponds to a pure multiphoton regime, in which the FTI process is very unlikely. We observed a monon-

tonic growth of the xFID signal with intensity, consistent with the suppression of the FTI contribution to the Rydberg population and the disappearance of the quantum interference. Above the ionization threshold, the REMPE shows a much smoother increase with intensity, very similar to H13. This means that the REMPE does not result from an interference process, but is dominated by a single mechanism, which is most probably a multiphoton resonantly-enhanced excitation process followed by radiative recombination.

Further information on the emission of xFID and REMPE can be obtained by studying the far-field spatial profile (Fig. 2 (b-e)). Above the ionization threshold, two quantum paths can generally contribute to HHG (short (s) and long (l) trajectories). They exhibit fairly different divergence properties, due to their different atomic dipole phase. The latter can be written $\phi_q^{l,s}(r, t) = -\alpha_q^{l,s} \cdot I_0(r, t)$, where $\alpha_q^{l,s}$ is a coefficient characteristic of the electron path in the continuum, and $I_0(r, t)$ is the temporally and spatially varying laser intensity. If the electron spends a long time in the continuum, $\alpha_q^{l,s}$ is high and the harmonics show a broad divergence, which rapidly increases with intensity. This is absolutely not the case for the above-threshold harmonics in our measurement. Their emission is very colimated, with ≈ 1 mrad divergence while the a fundamental laser divergence is above 10 mrad. Furthermore, they hardly show any spatial broadening as the laser intensity increases. This means that they are emitted by very short trajectories for which $\alpha_q^s \approx 0$. Below the ionization threshold, H9 show an increase of divergence between 2.5 to 3.5×10^{13} W/cm². This intensity range corresponds to the constructive interference between the two generating mechanisms (multiphoton and long trajectories) which could lead to a broader spatial profile due to the contribution of the latter. Last, the resonant components, and in particular the xFID, show a very strong divergence increase with driving laser intensity, suggesting the existence of a significant intensity-dependence of the initial phase of the emission process.

Several properties of below-threshold resonant harmonics make them potentially very appealing for applications. They can be very bright, and the photon yield does not saturate with increasing gas density until very high pressure are reached, which enables high conversion efficiency [11]. Furthermore, resonant HHG produced by elliptical laser pulses in argon are quasi-circularly polarized [10], opening new perspectives for ultrafast tabletop XUV circular dichroism experiments. The temporal characteristics of the resonant emission are thus extremely important. On one hand, Chini *et al.* claimed that double optical gating could be used to temporally gate the enhanced HHG emission by Rydberg states [11]. On the other hand, recent theoretical calculation of Camp *et al.* demonstrated that the narrow-band emission at Rydberg field-free energies was produced by dipoles ring-

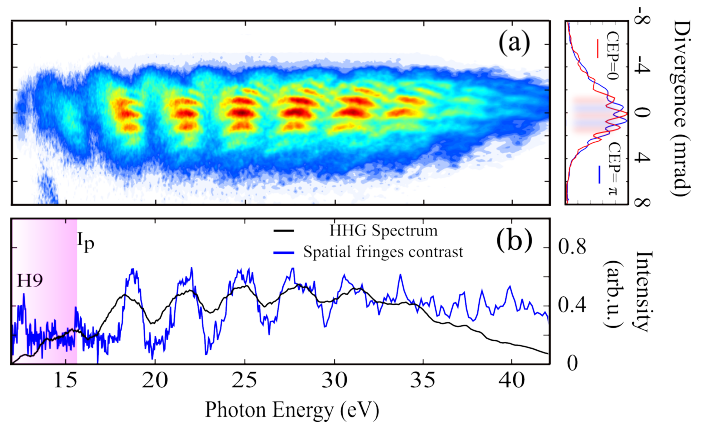


FIG. 3. Time-frequency mapping of HHG using the attosecond lighthouse technique. (a) Spatially-resolved harmonic spectrum driven by a spatially chirped laser pulse. (b) Spatially integrated harmonic spectrum (black dashed) and contrast of the spatial fringes (blue continuous). (c) Spectrally integrated harmonic spatial profile for two CEP values

ing for a time much longer than the generating pulse duration [13]. To tackle the question of the possible sub-cycle temporal confinement of the resonant XUV emission, we used the attosecond lighthouse technique [17].

The attosecond lighthouse technique consists in spatially separating different attosecond pulses from an attosecond pulse train using an ultrafast rotation of the laser wavefront at the focus. Each pulse of the attosecond pulse train is emitted in the direction orthogonal to the instantaneous wavefront. If the wavefront rotates fast enough, then two consecutive attosecond pulses are sent to different direction and separated on the detector in the far-field. Up to now, this technique has only been used with laser sources whose carrier-envelope phase (CEP) was stabilized, because changes of the CEP shift the position of the attosecond pulses on the detector [26]. To avoid using a CEP-stabilized laser source, we performed single-shot acquisitions of the harmonic spectrum, with a 1 ms exposure time on the CCD camera. Above threshold, clear fringes appear along the vertical dimension of the detector. From one laser shot to the next, the fringe pattern is found to shift, reflecting the fluctuations of the CEP. We recorded a series of images in these conditions, and tagged the CEP by measuring the phase of the spatial fringes by Fourier transform. We sorted the resulting images in CEP bins with $-300 \text{ mrad} < \phi_{CEP} < 300 \text{ mrad}$ acceptance.

Figure 3(a) shows the spatially streaked harmonic spectrum obtained using the attosecond lighthouse and averaged over 10 laser shots with the same CEP (± 300 mrad). Well separated horizontal fringes are visible. They shift vertically as the CEP changes, as illustrated in Fig. 3(b). Note that this is the first demonstration of single-shot CEP tagging of a CEP unstabilized

laser using attosecond lighthouse. The level of sub-cycle temporal confinement of the harmonic emission can be evaluated by measuring the contrast of the spatial fringe pattern, using Fourier analysis. The results are shown in Fig. 3(b). Above threshold, the harmonics exhibit significant spatial fringes contrast, which is a signature of the sub-cycle (attosecond) confinement of their emission. On the other hand, this contrast falls down drastically below the ionization threshold, around the energy range of the xFID emission. As the photon energy further decreases, the contrast increases again around H9. The spatial fringe visible for below- and above-threshold HHG is a signature of their attosecond pulse train temporal profile. The fact that spectral fringe are observed indicates that the xFID emission is not confined on the attosecond time-scale.

In conclusion, we have performed a systematic investigation of the role and the potential of Rydberg resonances in HHG. We have found that two pathways interfere to populate the Rydberg states. We also demonstrated that Rydberg states can emit XUV radiation through Free Induction Decay or by a new REMPE process, in which the population of the Rydberg can be followed by subsequent absorption of additional photons, giving rise to emission at energies $E_{\Omega} = E_R^{(S)} + 2n\hbar\omega$. This mechanism may enable to transfer unique properties of resonant HHG, for example the possibility of producing quasi-circular polarization state, above the ionization threshold. We also performed the first attosecond lighthouse measurement without CEP stabilisation. By measuring the contrast of the spatial fringes, we have demonstrated that the xFID radiation is not temporally confined on the sub-cycle timescale, unlike the usual above-threshold non-resonant harmonics.

We thank V. Blanchet, B. Fabre, F. Quéré, J. Mauritsson and B. Pons for fruitful discussion, R. Bouillaud and L. Merzeau for technical assistance, and E. Constant and E. Mével for providing experimental apparatus. We acknowledge financial support of the European Union (LASERLAB-EUROPE II 228334 and LASERLAB-EUROPE 284464), the French National Research Agency (ANR), through ANR MISFITS and IdEx Bordeaux LAPHIA (ANR-10-IDEX-03-02, and the NSERC Vanier and Alexander Graham Bell Canada Graduate Scholarships.

-
- [1] M. Y. Kuchiev, *JETP* **45**, 404 (1987).
 [2] P. B. Corkum, *Physical Review Letters* **71**, 1994 (1993).
 [3] K. J. Schafer, B. Yang, L. F. DiMauro, and K. C. Kulander, *Phys. Rev. Lett.* **70**, 1599 (1993).
 [4] M. Lewenstein, P. Balcou, M. Y. Ivanov, A. LHuillier, and P. B. Corkum, *Physical Review A* **49**, 2117 (1994).
 [5] R. A. Ganeev, M. Suzuki, M. Baba, H. Kuroda, and T. Ozaki, *Optics Letters* **31**, 1699 (2006).
 [6] V. Strelkov, *Physical Review Letters* **104**, 123901 (2010).
 [7] J. Rothhardt, S. Hdrich, S. Demmler, M. Krebs, S. Fritzsche, J. Limpert, and A. Tnnermann, *Physical Review Letters* **112**, 233002 (2014).
 [8] S. Haessler, V. Strelkov, L. B. E. Bom, M. Khokhlova, O. Gobert, J.-F. Hergott, F. Lepetit, M. Perdrix, T. Ozaki, and P. Salières, *New Journal of Physics* **15**, 013051 (2013).
 [9] A. Ferré, A. E. Boguslavskiy, M. Dagan, V. Blanchet, B. D. Bruner, F. Burgy, A. Camper, D. Descamps, B. Fabre, N. Fedorov, J. Gaudin, G. Geoffroy, J. Mikosch, S. Patchkovskii, S. Petit, T. Ruchon, H. Soifer, D. Staedter, I. Wilkinson, A. Stolow, N. Dudovich, and Y. Mairesse, *Nature Communications* **6** (2015).
 [10] A. Ferré, C. Handschin, M. Dumergue, F. Burgy, A. Comby, D. Descamps, B. Fabre, G. Garcia, R. Généaux, L. Merceron, E. Mével, L. Nahon, S. Petit, B. Pons, D. Staedter, S. Weber, T. Ruchon, V. Blanchet, and Y. Mairesse, *Nat Photon* **9**, 93 (2015).
 [11] M. Chini, X. Wang, Y. Cheng, H. Wang, Y. Wu, E. Cunningham, P.-C. Li, J. Heslar, D. A. Telnov, S.-I. Chu, and Z. Chang, *Nature Photonics* **8**, 437 (2014).
 [12] I. J. Sola, E. Mével, L. Elouga, E. Constant, V. Strelkov, L. Poletto, P. Villoresi, E. Benedetti, J.-P. Caumes, S. Stagira, C. Vozzi, G. Sansone, and M. Nisoli, *Nature Physics* **2**, 319 (2006).
 [13] S. Camp, K. J. Schafer, and M. B. Gaarde, *Physical Review A* **92**, 013404 (2015).
 [14] S. Bengtsson, E. W. Larsen, D. Kroon, C. Arnold, A. L’Huillier, L. Rippe, and J. Mauritsson, in *Frontiers in Optics 2015* (Optical Society of America, 2015) p. FTh3A.2.
 [15] F. Bloch, *Physical Review* **70**, 460 (1946).
 [16] R. G. Brewer and R. L. Shoemaker, *Phys. Rev. A* **6**, 2001 (1972).
 [17] H. Vincenti and F. Quéré, *Physical Review Letters* **108**, 113904 (2012).
 [18] X.-B. Bian and A. D. Bandrauk, *Applied Sciences* **3**, 267 (2013).
 [19] D. C. Yost, T. R. Schibli, J. Ye, J. L. Tate, J. Hostetter, K. J. Schafer, and M. B. Gaarde, *Nature Physics* **5**, 815 (2009), arXiv: 0901.3768.
 [20] W.-H. Xiong, J.-W. Geng, J.-Y. Tang, L.-Y. Peng, and Q. Gong, *Physical Review Letters* **112**, 233001 (2014).
 [21] L. He, P. Lan, C. Zhai, Y. Li, Z. Wang, Q. Zhang, and P. Lu, *Physical Review A* **91**, 023428 (2015).
 [22] H. Soifer, P. Botheron, D. Shafir, A. Diner, O. Raz, B. Bruner, Y. Mairesse, B. Pons, and N. Dudovich, *Physical Review Letters* **105** (2010), 10.1103/PhysRevLett.105.143904.
 [23] C. F. de Morisson Faria, R. Kopold, W. Becker, and J. M. Rost, *Physical Review A* **65**, 023404 (2002).
 [24] T. Nubbemeyer, K. Gorling, A. Saenz, U. Eichmann, and W. Sandner, *Physical Review Letters* **101** (2008), 10.1103/PhysRevLett.101.233001.
 [25] A. S. Landsman, A. N. Pfeiffer, C. Hofmann, M. Smolarski, C. Cirelli, and U. Keller, *New Journal of Physics* **15**, 013001 (2013).
 [26] F. Quéré, H. Vincenti, A. Borot, S. Monchocé, T. J. Hammond, K. T. Kim, J. A. Wheeler, C. Zhang, T. Ruchon, T. Auguste, J. F. Hergott, D. M. Villeneuve, P. B. Corkum, and R. Lopez-Martens, *Journal of Physics B: Atomic, Molecular and Optical Physics* **47**, 124004 (2014).